Archiv für Elektrotechnik 76 (1993) 397–404

Archiv für Elektrotechnik

Coupled magneto-thermal field computation in three-phase gas insulated cables

Part 2: Calculation of ampacity and losses

V. Hatziathanassiou and **D. Labridis,** Thessaloniki, Greece

Contents: The calculation of ampacity and losses of three-phases gas insulated cables based on the FEM formulation which was developed in Part 1 is presented. Limitations of the common mesh for both problems (electromagnetic and thermal) are also presented. Comparisons with existing calculations are made. Results concerning the sensitivity of cable ampacity and losses to variations of design and environmental parameters (burial depth, ambient temperature, soil thermal conductivity, cable emissivities, heat transfer coefficient, sheath radius) are finally presented.

Berechnung des gekoppelten magnetisch-thermischen Feldes dreiphasiger gasisolierter Kabel

Teil 2: Berechnung der Stromtragefähigkeit und Verluste

Übersicht: Basierend auf dem in Teil 1 beschriebenen Lösungsansatz mit der Finite-Elemente-Methode wird die Berechnung der Stromtragefähigkeit und der Verluste eines dreiphasigen gasisolierten Kabels angegeben. Dabei wird auch auf die Grenzen bei Verwendung eines für beide Probleme (elektromagnetisches und thermisches Feld) gemeinsamen Gitternetzes eingegangen und ein Vergleich mit existierenden Berechnungsverfahren gemacht. Abschließend werden Ergebnisse bezüglich der Abhängigkeit der Stromtragefähigkeit und der Verluste von Konstruktions- und Umgebungsparametern (Verlegetiefe, Umgebungstemperatur, Wärmeleitfähigkeit des Bodens, Wärmeabstrahlung des Kabels, Wärmeübergangskoeffizient, Mantelradius) vorgestellt.

1 Introduction

The solution of the coupled magneto-thermal field in a three phase gas insulation cable is presented in this paper. The method used is the finite element formulation that has been analysed in Part 1. The proposed method takes into account the real geometry and the real electromagnetic and thermal properties of the involved materials. The given quantity is the rms of the measurable current flowing through each conductor and the result is the computation of the magnetic vector potential (MVP) and temperature field distributions. From the MVP distribution, the current density distribution and all the other performance quantities (losses, forces, inductances) of the cable may easily be obtained. From the temperature distribution, using a given maximum sheath temperature as a limitation, the ampacity of the cable is also easily determined.

A general-purpose finite element program has been developed, using the same mesh for the two diffusion problems but with different boundary conditions on each one. Calculations have been made for different load conditions as well as for different material properties. The results have been compared with analytical and empirical approaches and with measurements. The accuracy of the proposed method is shown to be excellent.

For all the references made to Part 1 of the paper the suffix [P1] is used, e.g. Fig. 2 [P1].

2 Limitations of the discretization area

Both the electromagnetic and the thermal field of an underground cable may be considered as unbounded fields. The boundary conditions (2b) [P1], (9) [P1], (10) [P1] and (11) [P1] prevail at infinity, i.e. the limit C of the two-dimensional region S in most cases is not in a finite distance from the field sources. The FEM has been used to solve unbounded field problems using two different approaches:

a) Extension of the discretization area (direct solution),
b) use of integral equations (Green's function).

In the first method, the unbounded region S is always geometrically truncated into a bounded one. This is accomplished by the introduction of an artificial boundary C that lies at a finite distance from the field sources. In order to achieve an acceptable accuracy, this large selected area has to be tested by repeated solutions for regions of varying size. A second difficulty is that the number of nodal points of the FEM tends to be large, leading to the solution of a large system of equations. In the second method, the unbounded region S is usually divided into a bounded region and an unbounded one. With the help of a special form of Green's function, the problem is restated in the unbounded region in terms of an integral equation. The method has been used in electromagnetic [1] and thermal [2, 3] field problems and seems to lead to accurate results. However, there are some difficulties in finding the problem dependent Green's function and in making the discretization compatible with existing finite element techniques. There are also some restrictions concerning the unbounded region: it must be

homogeneous and isotropic. The previous direct FEM solution of the three-phase gas insulation cable electromagnetic problem [4] and the presence in the literature of direct FEM solutions of thermal underground cable problems [5, 6] led to the adoption of the first method for the finite element discretization area. The disadvantage of the large number of equations that this method will introduce may be circumvented by the evolution of the speed and memory capabilities of the modern computers and by the mesh grading, i.e. by progressively increasing the size of the finite elements for areas further away from the field sources.

One of the advantages of the finite element formulation of the problem presented in Part 1 of this paper, is that the boundary conditions of the thermal problem and the homogeneous Dirichlet condition of the electromagnetic problem have to be imposed on the same curve C. So it is possible to use the same finite element mesh for both diffusion problems and to define the appropriate boundaries for the problem that is currently solved.

The thermal diffusion problem will be examined first, because the boundary conditions are more complicated here. As shown in Fig. 1, the three-phase cable is buried in depth D from ground surface. The soil around the cable sheath has a thermal conductivity k_e and the region under consideration S is enclosed by curve C. This curve consists of the straight lines AB, $B\Gamma$, $\Gamma\Delta$ and ΔA, so that

$$C = AB \cup B\Gamma \cup \Gamma\Delta \cup \Delta A \tag{1}$$

In the boundary AB the convective heat loss is specified, according to the boundary condition (11) [P1]. The parameters needed for the definition of this boundary condition are the ambient temperature T_∞ and the heat transfer coefficient h between soil surface and air. According to the definition (11) [P1], the boundary C_{AB} is of the type C_3. On the other three boundary lines $B\Gamma$, $\Gamma\Delta$ and ΔA the temperature T is specified, i.e. a constant temperature boundary is used according to (9) [P1]. However, this is an artificial boundary that lies at a finite distance from the field sources. This distance has to be determined so that the boundary $C_{B\Gamma\Delta A}$, which is of the type C_1 according to the definition (9) [P1], may be assumed unaffected by the heat sources of the problem.

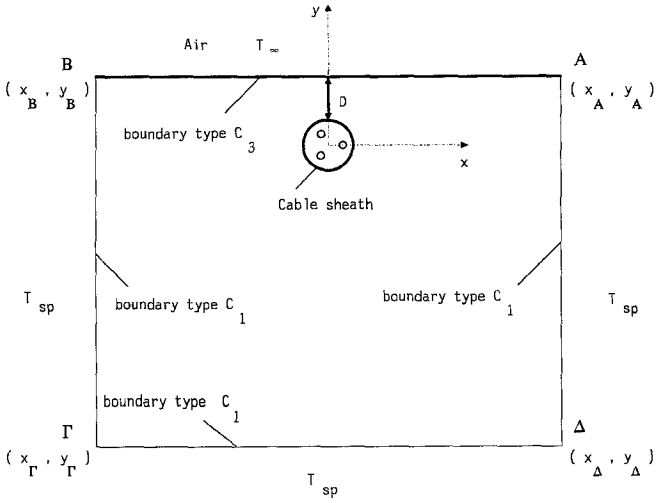

Fig. 1. Definition of the boundary conditions and of the size of the discretization area of the problem

The method of repeated solution has been adopted for the determination of the mesh size. The heat flux q_s per unit area at the boundary $C_{B\Gamma\Delta A}$ was computed in every new mesh, until this heat flux was equal to zero in every nodal point belonging to $C_{B\Gamma\Delta A}$. For this reason, a boundary condition of the type C_2 of (10b) [P1] has been originally used for the curve $C_{B\Gamma\Delta A}$ and the temperature of every node on this curve has been compared to a specified soil temperature T_{sp}. On the final mesh, a boundary condition of the type C_1 of (9) [P1] has been used for $C_{B\Gamma\Delta A}$ and the mean conductor and sheath temperatures T_c and T_s respectively were tested, as they were obtained with the use of the two different boundary conditions.

A typical three phase gas cable carrying an rms current of 2000 A has been considered buried at a depth $D = 0.5$ m and the quantities used for the boundary conditions were

$$\begin{aligned} T_\infty &= 15\,^\circ\mathrm{C} \\ T_{sp} &= 20\,^\circ\mathrm{C} \\ h &= 11.36\ \mathrm{W/^\circ C\ m^2} \end{aligned} \tag{2}$$

Because the points A and B lie on the ground surface and therefore their y-coordinates must be constant related to the buried cable (in the centre of which lies the origin of coordinates), the x- and y-coordinates of the other two points Γ and Δ so as the x-coordinates of the points A and B may vary. The repeated solutions along with the associated geometrical and physical data obtained are shown in Table 1. According to this table, the field was finally assumed to stretch 12 m on either side of the y axis and to a depth of 12 m below the x axis, in order to satisfy the zero heat flux condition on $C_{B\Gamma\Delta A}$. Subsequently the same mesh was used with boundary condition of the type C_1 on $C_{B\Gamma\Delta A}$ and the results are shown in Table 2. This

Table 1. Repeated solution for the determination of the optimum mesh size using boundary condition of type C_2 on $C_{B\Gamma\Delta A}$ and boundary condition of type C_1 on C_{AB}. The cable was buried in depth $D = 0.5$ m from soil surface as shown in Fig. 1.

$x_B = x_\Gamma$ [m]	$y_\Gamma = y_\Delta$ [m]	$x_A = x_\Delta$ [m]	$T - T_{sp}$ on $C_{B\Gamma\Delta A}$ [°C]		
			maximum	minimum	average
−3.0	−3.0	3.0	15.4	1.0	9.3
−6.0	−6.0	6.0	8.1	0.3	5.0
−12.0	−12.0	12.0	4.2	0.1	1.9

Table 2. Comparison of the results of the two FEM solutions using boundary condition of type C_2 and of the type C_1 on $C_{B\Gamma\Delta A}$, respectively. The boundary condition on C_{AB} is always of type C_3 (convective) and the final mesh of 24 m width and $12 + D + R_a$ m depth has been used.

boundary condition on $C_{B\Gamma\Delta A}$	mean sheath temperature T_s [°C]	mean conductor temperature T_c [°C]
type C_2, using (10b) [P1]	41.9	56.0
type C_1, using (9) [P1]	41.6	55.7

large mesh of a rectangular area of a width of 24 m and depth of $12 + D + R_a$ m (where R_a is the external sheath radius) is the final mesh that was used for all the remaining calculations in this paper. In the literature similar large meshes have been used for underground cable thermal calculations and their dimension vary from 6.1×6.1 m in [5] to 30.4×16.4 m in [6].

The satisfaction of the boundary conditions of the electromagnetic diffusion problem is the next question concerning the finite element mesh. The boundary condition that has to be imposed on C is the homogeneous Dirichlet condition obtained from (2b) [P1], i.e. using a zero value of $A_0(x, y)$ on C. The possible cases that can be met on the solution of power cables are the two following:

1. The cable sheath is made of a ferromagnetic material, for example steel sheaths, and
2. the cable sheath is made of a nonmagnetic material, for example aluminium sheath.

In the first case, due to the presence of the high permeability ferromagnetic material, the magnetic lines of flux are almost entirely confined to the cable sheath, so that the flux density is substantially zero outside the sheath. It is also known that in a 2dimensional problem the magnetic lines of flux are identical with the equipotentials of the magnetic vector potential (MVP). As a result, the artificial boundary C with a homogeneous Dirichlet condition may be located very near to the cable sheath without introducing any problems. In the second case, due to the nonmagnetic sheath, the MVP has nonzero values on the exterior of the cable sheath. However, due to the very low electric conductivity of the soil surrounding the sheath, in a short distance from the cable the MVP may be again assumed to be zero. This distance has been estimated [4] as 5 to 6 times a typical dimension of the cable, which on the case of a three phase gas cable may be assumed as the sheath radius R_i. Typical values for R_i are from 0.3 to 0.6 m, so the finite element mesh that has been already chosen for the satisfaction of the boundary conditions of the thermal problem automatically satisfies the electromagnetic boundary conditions. So in the boundary C of Fig. 1 the following conditions were imposed for the calculations:

Electromagnetic problem:

$$A_z|_C = 0$$

Thermal problem:

$$\text{on } C_{AB} \quad k\left[\frac{\partial T}{\partial x} l_x + \frac{\partial T}{\partial y} l_y\right] + h(T - T_\infty) = 0 \tag{3}$$

$$\text{on } C_{B\Gamma\Delta A} \quad T|_{C_{B\Gamma\Delta A}} = T_{sp}$$

3 Computation of losses and cable ampacity

The finite element iterative solution presented in Part 1 leads to the computation of the nodal values of the MVP A and the temperature T, as well as of the source current density J_{si} in conductor i (where in this case $i = 1, 2, 3$). Using these values, all the other performance quantities of the cable may be computed.

The total *ac* losses per unit length of the three phase gas cable are

$$P_t = 3P_c + P_s \quad [\text{W/m}] \tag{4}$$

where P_c and P_s are the *ac* losses per unit length of anyone of the three conductors and of the sheath, respectively. Defining an *ac* resistance per unit length of the cable R_{ac} such as

$$P_t = 3I_{rms}^2 R_{ac} \tag{5}$$

the *ac*/*dc* ratio will be

$$\frac{R_{ac}}{R_{dc}} = \frac{P_c}{P_{dc}} + \frac{P_s}{3P_{dc}} \tag{6}$$

where R_{dc} and P_{dc} are the *dc* resistance and *dc* loss, respectively, per unit length of a conductor, equal to

$$R_{dc} = \frac{1}{\pi(r_a^2 - r_i^2)\,\sigma_c} \quad [\Omega/\text{m}] \tag{7a}$$

and

$$P_{dc} = I_{rms}^2 R_{dc} \quad [\text{W/m}] \tag{7b}$$

From the conductivity definition as a function of temperature in (5) [P1], it is obvious that the *dc* quantities defined in (7) cannot be assigned a value before the end of the iterative solution. However, in order to have a constant quantity for reference, after the calculation of the mean temperature T_m^e of element e given by (15b) [P1], a mean temperature T_c of the three conductors is calculated. Using this temperature and (5) [P1], a mean conductor conductivity is defined by

$$\sigma_c = \frac{\sigma_{0c}}{1 + \alpha_c T_c} \quad [1/\Omega\text{m}] \tag{8}$$

and it is used for the definitions in (7) in every iteration.

Both sides of (6) may be calculated and therefore a verification of the accuracy of the solution may be accomplished. If a complex voltage drop per unit length of conductor i is defined as

$$V_i = \frac{J_{si}}{\sigma_c} \quad [\text{V/m}] \tag{9}$$

then the corresponding impedance per unit length of this conductor will be

$$Z_i = \frac{V_i}{I_{rms}} \quad [\Omega/\text{m}] \tag{10}$$

The real part of Z_i will be the ac resistance per unit length of conductor i, i.e.

$$R_{aci} = \text{Re}\,\{Z_i\} \quad [\Omega/\text{m}] \tag{11}$$

and because the conductors are symmetrically arranged, the *ac* resistance R_{ac} of the left side of (6) will be

$$R_{ac} = \frac{\sum_{i=1}^{3} R_{aci}}{3} = R_{aci}, \quad i = 1, 2, 3 \quad [\Omega/\text{m}] \tag{12}$$

For the evaluation of the quantities in the right side of (6) a distinction must be made between the conductor and the sheath losses. Consider first a typical finite element e lying on the cross-section of conductor i. The eddy current density J_e is given [4] in terms of the MVP A by

$$J_e = -j\omega\sigma A \quad [A/m^2] \tag{13}$$

so the relation between the corresponding element quantities will be

$$J_{ei}^e(x, y) = -j\omega\sigma A^e(x, y) \tag{14}$$

and the total current density distribution of element e may be obtained from

$$J_i^e(x, y) = J_{ei}^e(x, y) + J_{si} \tag{15}$$

Using (15) and symmetric quadrature formulae [7] of first degree it is easy to verify (16a) [P1]. Consider next a typical finite element e lying on the cross-section of the sheath. Then the source current density will be equal to zero, because the sheath carries no source current but only induced eddy currents and (16b) [P1] is obtained. So the average loss density contribution $\dot{q}^e$ of the typical element e defined in (14) [P1] can be easily calculated.

The mean value of the losses per unit length of element e will be obtained by the integration of $\dot{q}^e$ of this element S^e as

$$P^e = \iint_{S^e} \dot{q}^e \, dx \, dy \quad [W/m] \tag{16}$$

The integral in (16) can be expressed [4] using symmetric quadrature formulae of second degree. The total loss per unit length of conductor i is finally obtained from the summation of the element loss contribution of this conductor

$$P_{ci} = \sum_e P_{ci}^e, \quad i = 1, 2, 3 \quad [W/m] \tag{17a}$$

and the total loss per unit length of the sheath from the summation of the element loss contribution of the sheath

$$P_s = \sum_e P_s^e \quad [W/m] \tag{17b}$$

So the evaluation of the quantities in the right side of (6) is completed.

The mean temperatures of the conductors and of the sheath T_c and T_s, respectively, are calculated using the corresponding mean element values defined in (15b) [P1] and performing a summation over the conductors and sheath elements. The comparison of the values of T_c and T_s given by the FEM solution with the maximum permissible conductor and sheath temperatures leads to the estimation of the cable ampacity. Finally the MVP equipotentials of the electromagnetic field as well as the equitemperatural of the thermal field may be easily calculated and plotted, using the corresponding nodal values.

4 Results

4.1 Comparison with existing calculations

Graneau [8] presented an approximate ampacity computation of the 345 kV, 2020 A three phase gas cable proposed by Doepken [9]. In order to compute the maximum permissible current, he assumed a fixed sheath temperature of 60 °C and he used an iterative analytical and graphical method. The same cable has been examined with the FEM procedure presented in this paper and the results are shown in Table 3.

Table 3. Comparison of the loss and ampacity values of the FEM procedure with the corresponding values given in [8], for a specified mean sheath temperature T_s of 60 °C.

	T_s [°C]	P_c/P_{dc}	$P_s/3P_{dc}$	T_c [°C]	I_{rms} [A]
Computation of [8]	60.0	1.18	0.13	72.2	2148
FEM procedure	56.6	1.11	0.17	72.6	2148
(this paper)	60.0	1.11	0.17	77.5	2250

The differences encountered between the two solution originate from the approximations made by Graneau in order to accomplish a simple solution of the problem. For example, in order to compute the conductor *ac-dc* ratio, Graneau ignored the fact that the current distribution over the conductor cross section depends on the sheath induced eddy currents. He also considered the sheath eddy currents to be approximately half of the conductor currents. Due to the above approximations, his method leads to a total *ac-dc* ratio equal to 1.31, while the FEM coupled solution gives a total value of 1.28 and a lower sheath temperature T_s for the same rms current of 2148 A. In order to have the same sheath temperature of 60 °C, the FEM solution led to an ampacity of 2250 A.

For the next comparison of the FEM procedure the manufacturing data presented by Bolin et al. [10] have been used and the results are shown in Table 4. The current ratings used in [10] in order to achieve a 35 °C sheath temperature rise in soil of thermal conductivity $k_e = 1.11$ W/m °C, were used as input for the FEM procedure. The agreement of the *ac-dc* ratios as well as of the sheath temperature are excellent and the maximum difference in all tested cases is 4.9% in the losses and 11.1% in the temperature rise.

4.2 Parameter study of ampacity and losses

A three-phase gas insulated cable with geometrical and physical properties given by

$$\begin{aligned} r_a &= 0.063\,50 \text{ m} & d_c &= 0.012\,70 \text{ m} \\ R_i &= 0.342\,90 \text{ m} & d_s &= 0.012\,70 \text{ m} \\ m &= 0.299\,72 \text{ m} & & \\ \mu_{rc} &= 1 & \mu_{rs} &= 1 \\ \sigma_{c0} &= 3.86 \cdot 10^7 \text{ 1/}\Omega\text{m} & \sigma_{s0} &= 3.75 \cdot 10^7 \text{ 1/}\Omega\text{m} \\ \alpha_c &= 3.96 \cdot 10^{-3} \text{ 1/°C} & \alpha_s &= 3.96 \cdot 10^{-3} \text{ 1/°C} \end{aligned} \tag{18}$$

Table 4. Comparison of the total loss and temperature values of 5 different three-phase gas cables as obtained by the FEM procedure, with the corresponding manufacturing data of Bolin et al. [10]. The current ratings in [10] were measured for 35 °C sheath temperature rise above ambient temperature and with soil conductivity $k_e = 1.11$ W/m °C. In all cases the conductor wall thickness d_c was 0.012 7 m and the ambient temperature T_∞ was 20 °C (see Fig. 1 [P1] and Fig. 2 [P1] for symbols).

Voltage	I_{rms}	R_i	d_s	r_a	D	P_t from [10]	P_t from FEM procedure	$T_s - T_\infty$
[kV]	[A]	[m]	[m]	[m]	[m]	[W/m]	[W/m]	[°C]
145	1450	0.2476	0.0064	0.0445	0.8310	114.4	113.6	31.5
242	1650	0.2856	0.0064	0.0510	0.7750	121.6	126.4	32.7
362	2000	0.3479	0.0076	0.0635	0.7365	137.7	144.5	33.7
550	2550	0.4901	0.0114	0.0890	0.6665	154.8	150.8	31.1
800	2900	0.5575	0.0140	0.1015	0.6275	167.9	166.4	31.6

$$\begin{aligned} &\xi_c = 0.3 && \xi_s = 0.8 \\ &k_c = 150 \text{ W/m °C} && k_s = 150 \text{ W/m °C} \\ &k_a = 0.028 \text{ W/m °C} && k_e = 1.11 \text{ W/m °C} \\ &T_\infty = 20 \text{ °C} && T_{sp} = 20 \text{ °C} \\ &h = 11.36 \text{ W/m}^2 \text{ °C} && D = 0.50 \text{ m} \end{aligned} \tag{18}$$

(where all the symbols have been defined in Part 1) has been considered as a reference. For the calculations that follow, all the values of (18) are constant unless that single parameter which is explicitly declared.

In Figs. 2a, 2b the mean sheath and conductors temperatures T_s and T_c, respectively, have been calculated vs. rms current for 6 different depths D (from 0.25 to 1.50 m). As was expected, the cable ampacity decreases as the cable burial depth increases. If the sheath temperature has to be limited to 60 °C, the cable ampacity varies from 2190 A to 2900 A for a depth variation D from 1.50 m to 0.25 m respectively. Obviously, the ampacity sensitivity on burial depth variation is very strong.

In Figs. 3a, 3b mean sheath and conductors temperatures T_s and T_c have been calculated vs. rms current for different emissivity coefficients of sheath and conductors. For the same emissivity variations, the mean sheath temperature T_s is practically unaffected, while the mean conductors temperature T_c varies slightly.

The influence of the soil thermal conductivity k_e is shown in Figs. 4a, 4b. Both the sheath and conductors temperatures vary very strongly, as k_e changes from 0.5 W/m °C (dirt soil, clay, gravel) to 2.5 W/m °C (limestone, concrete). If the sheath temperature has to be limited to 60 °C, the cable ampacity varies from 1 830 A to 3000 A for a soil thermal conductivity k_e from 0.5 to 1.5 W/m °C.

The sensitivity of the cable ampacity on the ambient temperature T_∞ is shown in Figs. 5a, 5b. As the ambient temperature varies from 10 to 30 °C, the cable ampacity decreases from 2900 A to 2310 A, for the same limit $T_s = 60$ °C. The ampacity sensitivity on ambient temperature is also strong. On the contrary, the influence of the specified temperature T_{sp} on the cable ampacity is very weak. As shown from the corresponding Fig. 6, while T_{sp} varies from −5 to 20 °C, the temperature variation in both sheath and conductors is about 3.5%.

In Fig. 7 the effect of the heat transfer coefficient h between ground and air is shown. The sheath and conductor temperatures change rather slightly. With a change in h from 5 to 25 W/m² °C, the corresponding temperature variation is from 6% for low values of current to 11% for high values of I_{rms}.

The *ac-dc* loss ratio of the cable for all the cases examined in Fig. 2 to Fig. 7 is slightly influenced by the

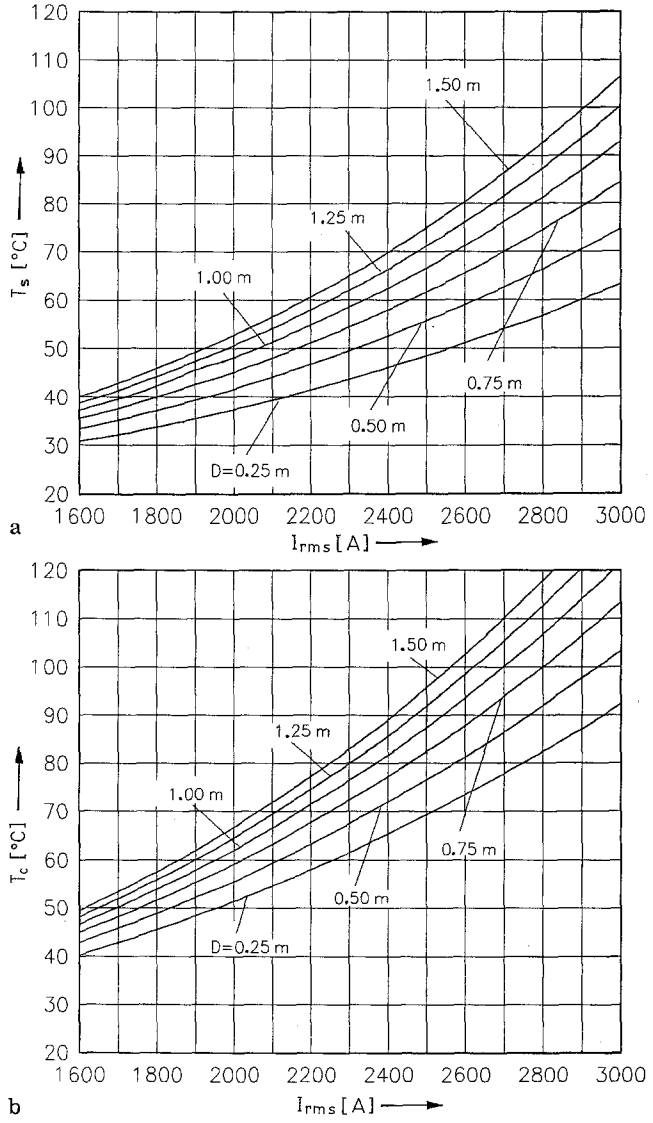

Fig. 2a, b. Sheath **(a)** and conductor **(b)** mean temperatures T_s and T_c, respectively, vs. rms load current for different depths D

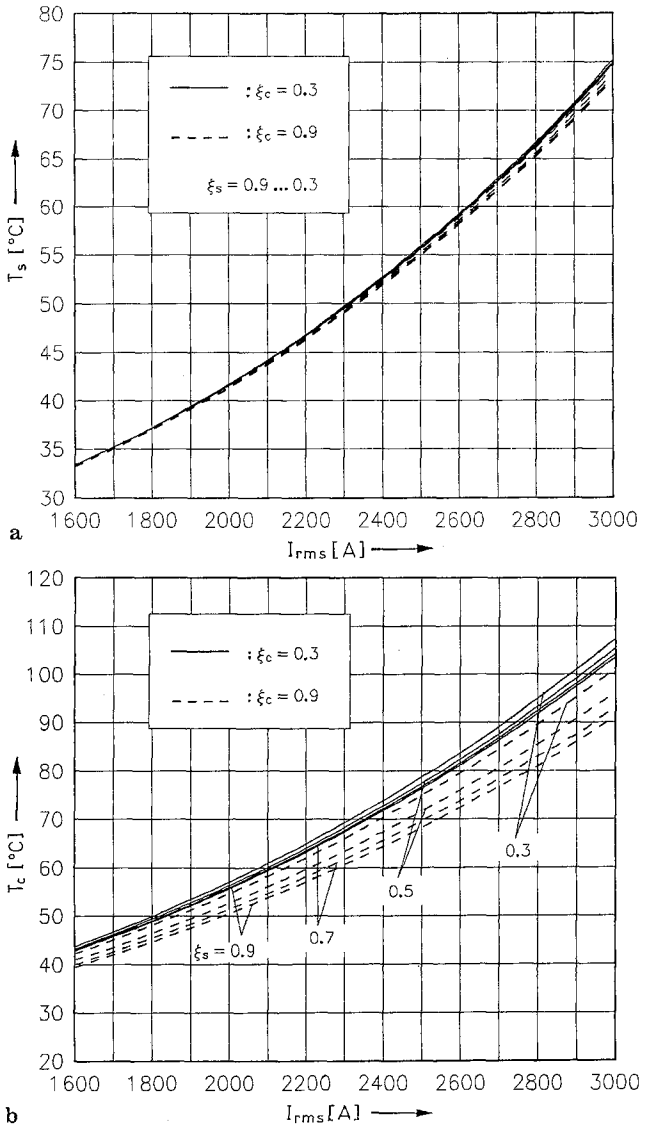

Fig. 3 a, b. Sheath **(a)** and conductor **(b)** mean temperatures T_s and T_c, respectively, vs. rms load current for different emissivities ξ_c and ξ_s

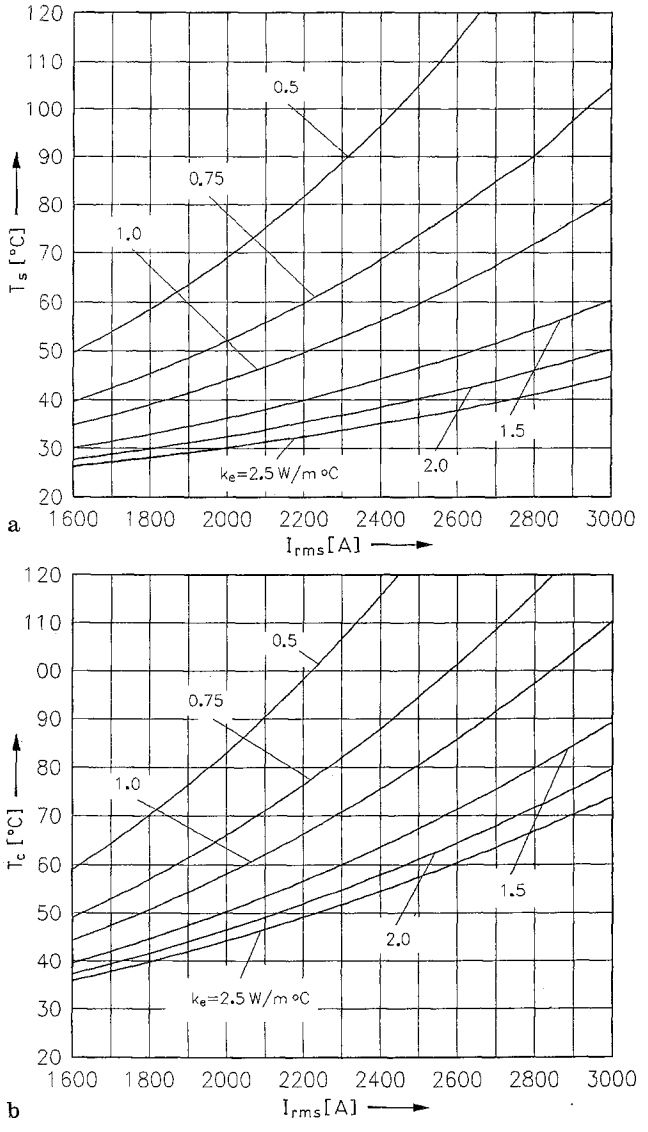

Fig. 4 a, b. Sheath **(a)** and conductor **(b)** mean temperatures T_s and T_c, respectively, vs. rms load current for different soil thermal conductivities k_e

parameter under investigation. The calculated values of the conductors and sheath loss ratios are about 1.12 and 0.17, respectively. Their variation, for all tested currents and depths, is less than 4%.

The sheath radius R_i is the next parameter, of which the influence on cable ampacity and losses is examined. In Figs. 8 a, 8 b the mean sheath and conductors temperatures T_s and T_c of the cable defined in (18) have been calculated vs. rms current for 6 different sheath radii R_i (from 0.26 to 0.36 m). The cable ampacity decreases strongly as the sheath radius decreases. For the same limitation of $T_s = 60\,°C$, the cable ampacity varies from 2680 A to 2080 A when the sheath radius decreases from 0.36 m to 0.26 m, respectively. This is also expected, because the sheath losses increase strongly as the sheath approaches the conductors. The effect of sheath radius on *ac-dc* loss ratio of the cable is shown in Fig. 9, where the loss ratio defined in (6) is plotted vs. rms current for the same variation of sheath radius R_i. To conclude, both the ampacity and losses sensitivity on sheath radius variation is very strong.

4.3 Computational remarks

The convergence of the iterative procedure presented in Part 1, used for the calculation of the quantity T_{err} a value of 1 °C, was very fast. The number of the required iterations is a function of the rms load current and of the original sheath T_{sa} and conductors T_{ca} temperatures chosen. All the tested cases needed at most 3 iterations. The discretization of the region S of Fig. 1 into finite elements is made automatically using Delaunay triangulation. Mesh grading has been used, in order to reduce the computer resources (computational time and memory) required for the iterative solution.

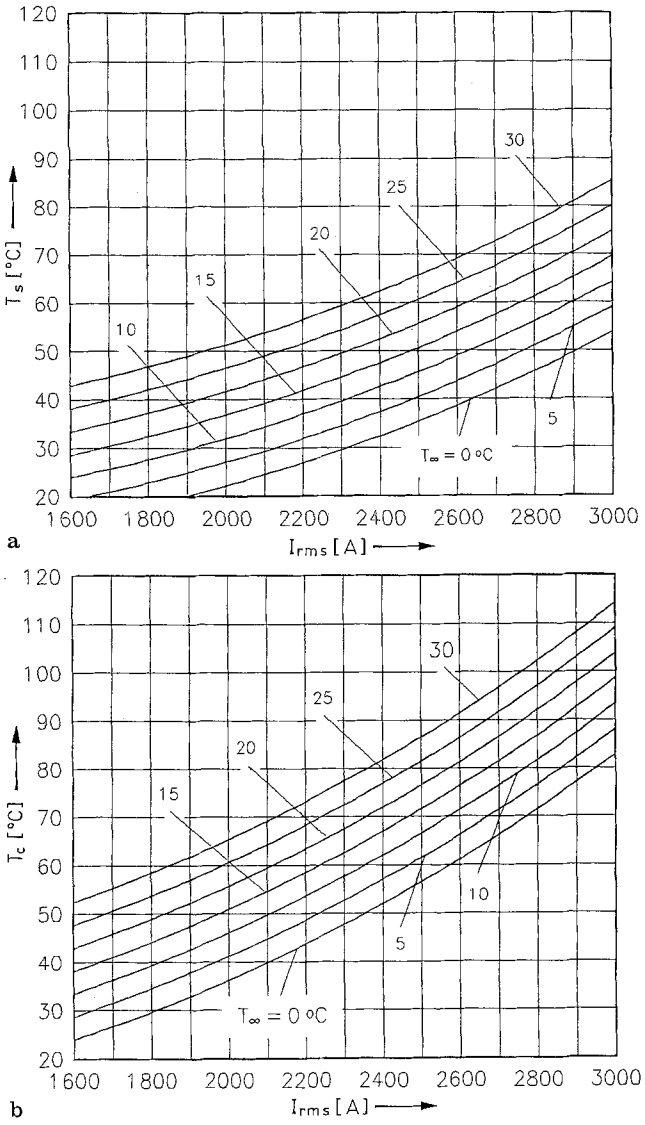

Fig. 5a, b. Sheath **(a)** and conductor **(b)** mean temperatures T_s and T_c, respectively, vs. rms load current for different air temperatures T_∞

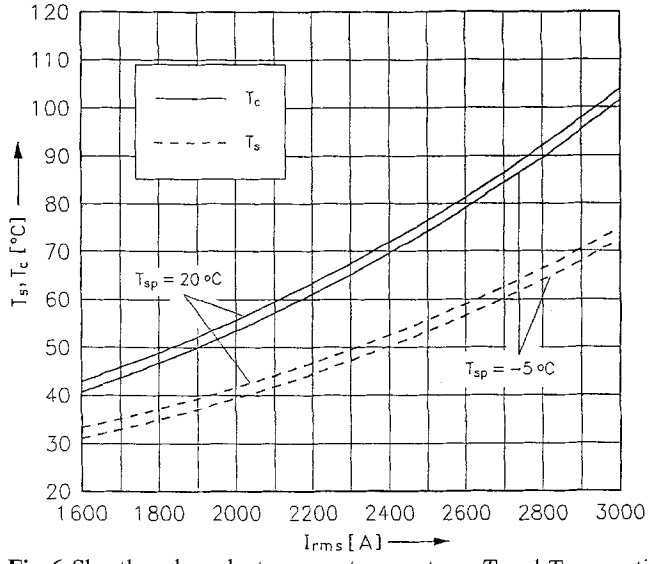

Fig. 6. Sheath and conductor mean temperatures T_s and T_c, respectively, vs. rms load current for different specified temperatures T_{sp} on curve $C_{B\Gamma\Delta A}$ of Fig. 1

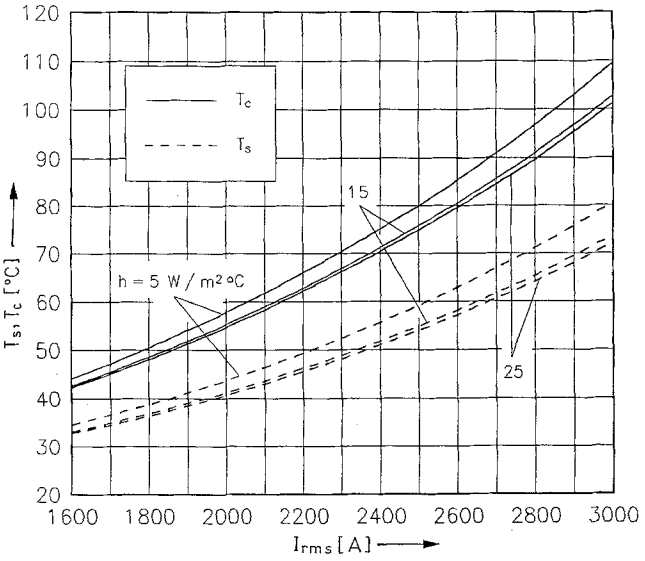

Fig. 7. Sheath and conductor mean temperatures T_s and T_c, respectively, vs. rms load current for different heat transfer coefficients h

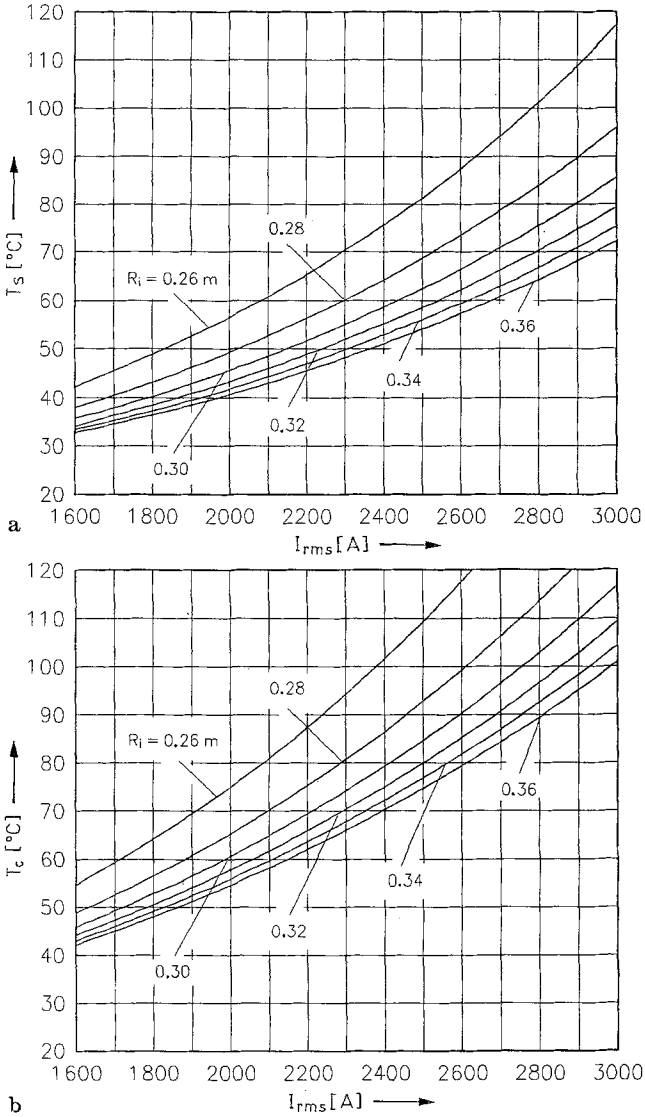

Fig. 8a, b. Sheath **(a)** and conductor **(b)** mean temperatures T_s and T_c, respectively, vs. rms load current for different sheath radii R_i

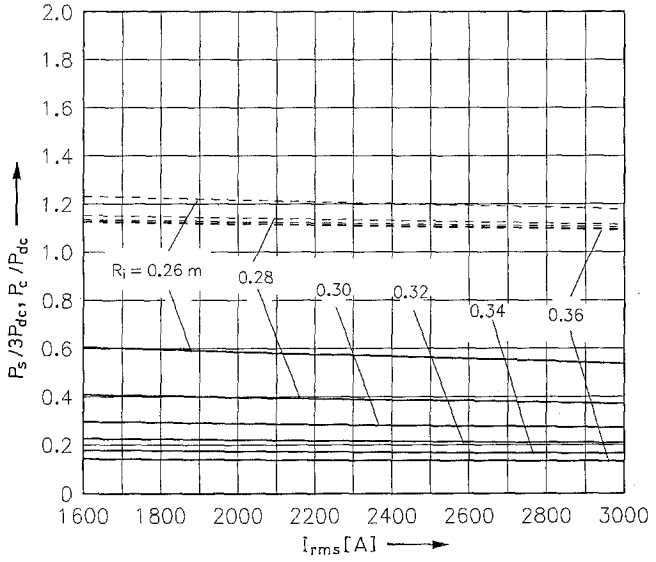

Fig. 9. Sheath (——) and conductor (– – –) loss ratios $P_s/3P_{dc}$ and P_c/P_{dc}, respectively, vs. rms load current for different sheath radii R_i

5 Conclusions

The iterative procedure using the finite element formulation presented in Part 1 has been used for the calculation of the ampacity and losses of a three-phase gas insulated cable. The validity of the method was confirmed by comparing with existing solutions as well as with measured data and the agreement was found to be excellent. Results for the sheath and conductors mean temperatures and loss ratios have been presented, using a variety of physical and geometrical data. The most important parameters that influence the cable ampacity are soil thermal conductivity, burial cable depth and ambient air temperature, while other parameters such as emissivities of cable materials or ambient soil temperatures have confined influence. The *ac* cable losses depend mainly on the geometrical and not on the thermal parameters. The method is capable to take into account any configuration of underground cables (using any geometrical and physical properties), surrounded by materials with different thermal conductivities as well as the effect of forced and seasonal cooling.

References

1. Silvester, P.; Hsieh, M.-S.: Finite element solution of 2dimensional exterior field problems. IEE Proc. Vol. 118 (1971) 1734–1747
2. Sroka, J.: The finite element method in unbounded temperature field of power cables. Arch. Elektrotech. 67 (1984) 1–4
3. Tarasiewicz, E.; Kuffel, E.; Grzybowski, S.: Calculation of temperature distribution within cable trench backfill and the surrounding soil. IEEE Trans. Power Appar. Syst. 104 (1985) 1973–1978
4. Labridis, D.; Dokopoulos, P.: Finite element computation of field, losses and forces in a three-phase gas cable with nonsymmetrical conductor arrangement. IEEE Trans. Power Delivery 3 (1988) 1326–1333
5. Mitchell, J.; Abdel-Hadi, O.: Temperature distribution around buried cables. IEEE Trans. Power Appar. Syst. 98 (1979) 1158–1166
6. Kellow, M. A.: A numerical procedure for the calculation of the temperature rise and ampacity of underground cables. IEEE Trans. Power Appar. Syst. 100 (1981) 3322–3330
7. Silvester, P.: Symmetric quadrature formulae for simplexes. Math. of Computation 24 (1970) 95–100
8. Graneau, P.: Underground power transmission. New York: John Wiley & Sons 1979
9. Doepken, H. C.: Compressed gas insulated cables with increased ampacity and reduced cost. Underground T and D Conference (1974) 536–540
10. Bolin, P. C.; Cookson, A. H.; Hopkins, M. D.; Corbett, J. T.; Marchlewski, J. H.; Hoscila, G. A.; Shimsock, J. F.: Manufacture and installation of a three conductor SF_6 insulated transmission line. IEEE Trans. Power Appar. Syst. 101 (1982) 1966–1974

Received July 28, 1992

V. Hatziathanassiou

D. Labridis

Aristotelian University of Thessaloniki
Department of Electrical Engineering
Section of Electrical Energy
P.O. Box 486
54006 Thessaloniki
Greece